TOXICOLOGICAL SCIENCES 44, 80–86 (1998)
ARTICLE NO. TX982476

A Multiple-Path Model of Fiber Deposition in the Rat Lung

Bahman Asgharian*,[1] and Satish Anjilvel†

*Chemical Industry Institute of Toxicology, Research Triangle Park, North Carolina 27709-2137; and †Department of Neuroscience, New York State Psychiatric Institute, New York, New York 10032

January 12, 1998; accepted April 10, 1998

A Multiple-Path Model of Fiber Deposition in the Rat Lung. Asgharian, B., and Anjilvel, S. (1998). *Toxicol. Sci.* 44, 80–86.

An asymmetric multiple-path model of particle deposition in the lung airways developed previously (S. Anjilvel and B. Asgharian, 1995, *Fundam. Appl. Toxicol.* 28, 41–50), was extended to calculate deposition of fibers in the rat lung by replacing the deposition efficiency expressions for particles with those of fibers. The effects of various parameters such as breathing parameters or fiber dimensions on deposition were studied. Fiber deposition fraction for one single breath was calculated per acini, lobe, and region of interest in the lung. The results were compared with one other model prediction and with data available in the literature. Good agreement between the model predictions and other studies was found. © 1998 Society of Toxicology.

Fibrous materials have been widely used in industry. People have been exposed to these materials. Once inhaled, fibers may deposit in the lung and create disease in the bronchial tree, small airways, and pleural region (Coin *et al.*, 1992). The difficulties associated with conducting experiments to determine fiber deposition in the lung have made mathematical models a convenient and desirable means of assessing dose/risk associated with exposure to different levels of fibers. A realistic lung dosimetry model for deposition can aid in understanding the underlying processes that inhaled fibers go through in the lung and the sites and amount of deposition. Deposition models are particularly useful for predicting dose to regions of the human lung where experimental measurement is not feasible.

A few models of fiber deposition in the respiratory tract are available. These models assume the lung to be made of three compartments (the head, tracheobronchial, and pulmonary regions) (Beeckmans, 1972; Harris and Fraser, 1976) or to have a single-path, dichotomous geometry representing an average lung airway (Asgharian and Yu, 1988, 1989; Ding *et al.*, 1997). These models are useful for the prediction of regional deposition in the lung. However, they do not generate reliable information regarding dose distribution within a region or deposition within a lobe since detailed anatomical structure of lung geometry is not provided.

This study uses a multiple-path model dosimetry model for predicting particle deposition in the rat lung that was developed previously by Anjilvel and Asgharian (1995). The mathematical approach of the model is similar to that of the single-path model (Yu, 1978). However, the major advantage of the multiple-path model is that it makes use of actual lung measurement data and thus incorporates the asymmetric feature of the lung. The monopodial feature of the rat lung makes spherical particle or fiber deposition in the lung highly dependent on the branching pattern of the lung airways. In addition, each terminal bronchial has a separate acinus attached to it; as a result, the dose in each acinus varies since it is located on a different airway pathway and is at a different distance from the trachea. The multiple-path model allows deposition calculations among different acini and thus predicts the dose distribution within a region.

The multiple-path deposition model developed originally for particles was modified and extended to fibers for calculating the deposition fraction of fibers in the rat lung. The influence of lung structure, breathing parameters, and fiber size on the deposition were investigated.

Deposition models need to be verified by comparing their predictions with available experimental data. The model was verified by comparing its predictions with one other predictive model and with available experimental data on the initial deposition of fibers on lung airway surfaces (Evans *et al.*, 1973; Griffis *et al.*, 1981; Morgan *et al.* 1978; Roggli and Brody, 1984). The calculations were performed for polydisperse fibers of the sizes given in each experimental study. Where information was not available (e.g., animal breathing parameters), reported values from the literature were used in the calculations.

MODEL DESCRIPTION

Lung Structure

The lung data used were that measured by Raabe *et al.* (1977) at the Lovelace Foundation for Medical Education and Research. The airway measurements were taken from the lung casts of Long-Evans rats. The data comprised the branching structure of the tracheobronchial tree and the length, diameter, branching angle, and gravity (orientation) angle of each airway. Overall, there were 4807 conducting airways with 2404 terminal bronchioles.

In the current study, each terminal bronchial was followed by an eight-

[1] To whom correspondence should be addressed at CIIT, 6 Davis Drive, P.O. Box 12137, Research Triangle Park, NC 27709-2137. Fax: (919) 558-1300. E-mail: asgharian@ciit.org.

1096-6080/98 $25 00

generation symmetric acinus similar to that by Yeh *et al.* (1979). The acini were assumed to have the same structure and volume.

Head Deposition

Deposition in the head region is mainly by impaction and diffusion. No experimental data are available on the deposition of fibers in the head region of the rat. For this reason, the results for spherical particles are extended to fibers by including the effects of fiber geometry and orientation. Due to the complex geometry of the nasal region and high air flow rate in this region, fiber orientation was assumed to be random. For impaction losses, the equation suggested by Zhang and Yu (1993) is employed.

$$\eta_{hi} = \left[\frac{(\chi)^{2.553}}{10^5 + (\chi)^{2.553}}\right]^{0.627}, \quad (1)$$

where χ is related to Fiber Stokes number.

$$\chi = \frac{1}{3}\left(\frac{d_f}{d_f} C_{\parallel} + 2\frac{d_f}{d_{f_\perp}} C_{\perp}\right)\rho d_f^2 \beta Q, \quad (2)$$

in which ρ, d_f, and β are fiber mass density, diameter, and aspect ratio (ratio of fiber length to fiber diameter) respectively, and d_f and $d_{f_\perp}$ are Stokes diameters, Q is the inhalation flow rate, and $C_{\parallel}$ and $C_{\perp}$ are slip correction factors given by Asgharian *et al.* (1988).

Losses by diffusion in the nasal region of the rat are given by Ding *et al.* (1997).

$$\eta_{hd} = 1 - \exp(-19.76 D^{1/2} Q^{-1/8}), \quad (3)$$

where D is the fiber diffusion coefficient.

$$D = \frac{\kappa T}{3\pi\mu d_f}\left(\frac{1}{3}\frac{d_f}{d_f} C_{\parallel} + 2\frac{d_f}{d_{f_\perp}} C_{\perp}\right), \quad (4)$$

in which κ is the Boltzmann constant, T is the absolute temperature, and μ is the air viscosity. The overall nasal deposition efficiency can be written as

$$\eta_h = 1 - (1 - \eta_{hi})(1 - \eta_{hd}). \quad (5)$$

Deposition Efficiencies in the Lung

Fiber deposition depends strongly on its orientation in the flow field. Fiber orientation can change while traveling in the airway, adding to the complexity of the analysis. Asgharian (1988) and Asgharian and Yu (1989) showed that fibers traveling in the lung airway assume a definite orientation depending on the acting loss mechanisms. For small fibers for which diffusion is the dominant loss mechanism, fibers may be assumed to be oriented randomly. On the other hand, for sedimentation and impaction losses that occur for large fibers, the fibers may be assumed to align in the direction of the flow.

Fibers may deposit in the lung airway by the combined mechanisms of sedimentation, diffusion, and impaction. When a fiber moves near a wall, it may also deposit by interception. Sedimentation and diffusion losses occur while the fiber is traveling along an airway. Impaction losses, on the other hand, take place primarily near a bifurcation when the incoming air turns but the suspended fibers in the air are unable to follow the streamlines due to their inertia and as a result may impact on the side walls of the airways. Below are the deposition efficiency equations used in the deposition calculations.

Diffusion. Constant collision of the fibrous particles with air molecules creates a Brownian motion that may lead to fiber deposition on the lung airways. This mechanism is significant for small, light fibers and occurs in the small airways of the lung where the air flow rate is small and the flow is parabolic. Ingham (1975) derived an expression for diffusion loss of particles in a parabolic flow.

$$\eta = 1 - 0.819\exp(-14.63\Lambda) - 0.097\exp(-89.22\Lambda) - 0.0325\exp(-228\Lambda) - 0.0509\exp(-125.9\Lambda^{2/3}), \quad (6)$$

where

$$\Lambda = \frac{LD}{4UR^2}, \quad (7)$$

in which L and R are, respectively, the airway length and radius, and U is the average airflow velocity in the airway. Diffusion coefficient D is calculated from Eq. (4).

Sedimentation. The gravitational settling of fibers in an airway is obtained from Wang (1975). It is significant in small airways of the lung. Fibers align quickly in the direction of the flow in these airways. If α is the inclination angle of the airway with respect to the horizontal, the following equations are used to calculate sedimentation losses depending on whether the flow is upward or downward:

When the flow travels upward, three cases can occur depending on the value of α.

For

$$0 < \alpha < \frac{\pi}{2} - \frac{2R}{9L}\left(\frac{2\nu_s}{3U}\right)^{1/2}$$

$$\eta_s = \frac{1}{\pi}\left(3\sqrt{\sigma(1-\sigma)} + \sin^{-1}\sqrt{1-\sigma} + (1-9\sigma^2)\sin^{-1}\sqrt{\frac{1-\sigma}{1+3\sigma}}\right) - \frac{2}{\pi}\left(\sqrt{\gamma(1-\gamma)}(1-2\gamma) + \sin^{-1}\sqrt{1-\gamma}\right), \quad (8)$$

where

$$\gamma = \frac{\left(\frac{3\nu_s L}{8UR}\cos\alpha\right)^{2/3}}{\left(1 - \frac{\nu_s}{2U}\sin\alpha\right)} \quad (9)$$

and

$$\sigma = \frac{\frac{\nu_s}{6U}\sin\alpha}{\left(1 - \frac{\nu_s}{2U}\sin\alpha\right)}, \quad (10)$$

in which ν_s is the gravitational settling velocity when the fibers are aligned to the flow.

For

$$\frac{\pi}{2} - \frac{2R}{9L}\left(\frac{2\nu_s}{3U}\right)^{1/2} < \alpha < \frac{\pi}{2} - \frac{R\nu_s}{8UL}$$

$$\eta_s = \frac{1+3\sigma}{\pi}\sqrt{1-\zeta_0^2}\left(\zeta_0 + \frac{4\gamma^{3/2}}{\sqrt{1+3\sigma}} - \sqrt{\zeta_0^2 - \frac{3\sigma}{1+3\sigma}}\right) + \frac{1-9\sigma^2}{\pi}\sin^{-1}\sqrt{1-\zeta_0^2} - \frac{1}{\pi}\sin^{-1}\sqrt{(1+3\sigma)(1-\zeta_0^2)}, \quad (11)$$

where

$$\zeta_0 = \frac{R\nu_s \sin^2\alpha}{8UL\cos\alpha} - \frac{1}{16}\sqrt{\frac{\nu_s}{6U}}\sin\alpha + \frac{7L}{8R}\cot\alpha. \quad (12)$$

For

$$\alpha > \frac{\pi}{2} - \frac{R\nu_s}{8UL}, \quad \eta_s = 0 \quad (13)$$

For the flow traveling downward, the following expression is used to calculate deposition efficiency:

$$\eta_s = 1 - \frac{2}{\pi}\sin^{-1}\sqrt{1-\zeta_1^2} + \frac{\sqrt{1-\zeta_1^2}}{\pi\left(1+\frac{\nu_s}{U}\sin\alpha\right)} \times \left(\frac{3\nu_s L}{2UR}\cos\alpha - \left(2+\frac{\nu_s}{U}\sin\alpha\right)\zeta_1\right), \quad (14)$$

where

$$\zeta_1 = \left(\frac{\frac{3\nu_s L}{8UR}\cos\alpha}{1+\frac{3\nu_s}{4U}\sin\alpha}\right)^{1/3}. \quad (15)$$

Impaction. This loss mechanism is significant in the lung upper airways where fibers are nearly aligned to the flow. The deposition efficiency by impaction is given by Cai and Yu (1988).

$$\eta_i = G(\theta, R/R_0) \times \mathrm{Stk}, \quad (16)$$

where θ is the bifurcation angle, R_0 and R are the parent and daughter radius respectively, and Stk is the Stokes number.

$$\mathrm{Stk} = \frac{C_1\rho d_f^2\beta U}{36\mu d_f R_0} \quad (17)$$

$$G(\theta, R/R_0) = \frac{8\sin\theta f_1(\theta, R/R_0)}{(R/R_0) f_0(\theta, R/R_0)} \quad (18)$$

$$f_0(\theta, R/R_0) = \pi\left[1 - \frac{1}{4}\left(\frac{R}{R_0}\right)^2\right] - \frac{4}{3}\left(\frac{15}{16}\pi - 2\right)\left(\frac{R}{R_0}\right)^2\cos^2\theta \quad (19)$$

$$f_1(\theta, R/R_0) = 1 - \frac{1}{3}\left(\frac{R}{R_0}\right)^2 + \left(\pi - \frac{11}{3}\right)\left(\frac{R}{R_0}\right)^2\cos^2\theta - \frac{1}{3}\left(\frac{R}{R_0}\right)^2\sin\alpha\left(\frac{2}{3} - \frac{\pi}{8}\right)\left(\frac{R}{R_0}\right)^4\cos^2\theta + \frac{1}{5}\left(\frac{R}{R_0}\right)^4\sin^2\theta + \left(6 - \frac{15}{8}\pi\right)\left(\frac{R}{R_0}\right)^4\cos^4\theta + \left(\frac{7}{15} - \frac{\pi}{8}\right)\left(\frac{R}{R_0}\right)^4\sin^2\theta\cos^2\theta. \quad (20)$$

Deposition Model

The flow in an airway was assumed to be uniform and traveling at the average parabolic velocity for that airway. The flow partitioning in each airway was proportional to its distal volume. The flow rates and the time when the inspiratory front of fresh air crosses the proximal and distal ends of an airway were determined. Aerosol concentrations at the proximal and distal ends of each individual airway were calculated using deposition efficiencies to account for losses in each airway. Deposited mass in each airway was computed using the principle of mass balance.

$$m_{dep} = m_{ini} + m_{in} - m_{out} - m_{rem}, \quad (21)$$

where, m_{dep} is the mass deposited in an airway, m_{in} is the mass initially in the airway, m_{in} and m_{out} are the masses entering and leaving the airway, and m_{rem} is the undeposited mass in the airway. Mass entering or leaving an airway is calculated from the expression

$$m_{in} \quad \text{or} \quad m_{out} = \int_0^T qC(t)dt, \quad (22)$$

where q is the flow rate through the airway, $C(t)$ is the aerosol concentration at the entrance or exit of the airway, and T is the breathing period. There is no pause between inhalation and exhalation. The mass of airborne fibers remaining at the end of inhalation is equal to the initial mass of the airborne fibers at the beginning of exhalation and is given by

$$m_{rem} \quad \text{or} \quad m_{ini} = A\int_0^L C(x)dx, \quad (23)$$

where A is the airway cross-sectional area and x is the distance along the airway. There are no airborne fibers at the start of inhalation or at the end of exhalation in the airways. The details of the model are described in Anjilvel and Asgharian (1995).

RESULTS

Calculations were performed using the Lovelace data to represent the dimensions at total lung capacity (Raabe *et al.*, 1977). A breathing rate of 150 breaths per minute and a tidal volume of 1.67 cm^3 was chosen. Fiber density was assumed to be 3.37 g/cm^3. For the model calculations, head region was omitted (i.e., fibers enter through the trachea). Head deposition was included only when the calculated results were compared with experimental data. The head region was added only when the results were compared with available experimental data in the literature.

Deposition of fibers entering the trachea in the tracheobronchial region of the rat lung is shown in Fig. 1. Fibers with diameters smaller than 0.1 μm appear to deposit by diffusion, while those larger than 0.2 μm deposit by impaction. The minimum deposition where both impaction and diffusion are small occurs near 0.2 μm fiber diameter and varies with fiber aspect ratio. The larger the aspect ratio, the smaller is the diameter. For a given fiber diameter, deposition fraction decreases with aspect ratio in the diffusion range and increases with aspect ratio in the impaction range.

Deposition of fibers entering the trachea in the alveolar region is shown in Fig. 2. The flow rate in this region is small, and, as a result, fiber deposition occurs by diffusion for small fibers and sedimentation for large ones. Due to the filtering effect of the tracheobronchial region, the deposition fraction in

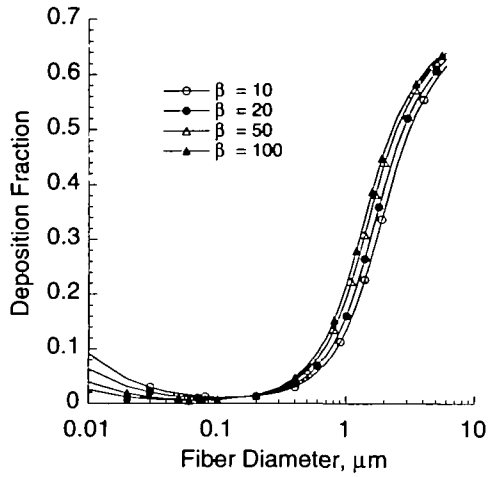

FIG. 1. Fraction of particles entering the trachea that deposited in the tracheobronchial region for a tidal volume of 1.67 cm^3 and breathing frequency of 150 min^{-1}. Fiber density was 3.37 g/cm^3.

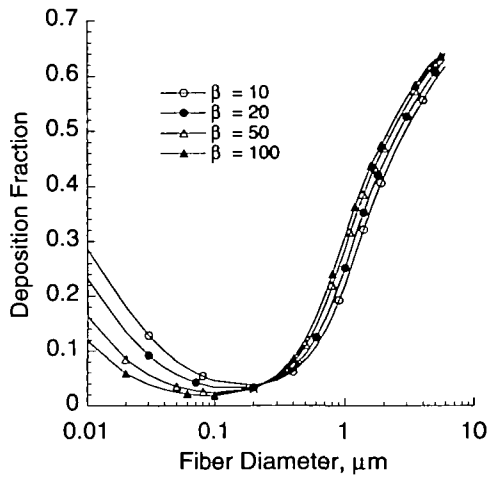

FIG. 3. Fraction of particles entering the trachea that deposited in the lower respiratory tract (tracheobronchial + alveolar) for a tidal volume of 1.67 cm^3 and breathing frequency of 150 min^{-1}. Fiber density was 3.37 g/cm^3.

the alveolar region shows two peaks, one in the diffusion range (not shown here) and a second peak near 1 μm in the sedimentation range. In the diffusion range, fiber deposition increases with decreasing aspect ratio. Fiber deposition by sedimentation increases weakly with increasing aspect ratio for fiber diameter less than 1 μm and decreases with increasing aspect ratio for fiber diameter larger than 1 μm.

Deposition of fibers entering the trachea in the lower respiratory tract (i.e., tracheobronchial plus alveolar region) when head deposition is neglected is shown in Fig. 3. The shape of the curves are similar to that for tracheobronchial region except for an inflection point around 1 μm diameter. Deposition fraction in the lower respiratory tract decreases with increasing fiber aspect ratio when losses are due to diffusion and increases with aspect ratio when losses are due to sedimentation and impaction. The diameter range at which losses are minimal in the alveolar region is similar to that in the tracheobronchial region.

A major advantage of the multiple-path model is that it can predict deposition at a specific site in the lung. The deposition fraction of fibers entering the trachea in various lobes of the lung, including right diaphragmatic (RD), right intercostal (RI), right apical (RA), right cardiac (RC), left diaphgragmatic (LD), and left apical (LA), is shown in Fig. 4. The deposition fraction in each lobe includes those fibers deposited in the acini plus those deposited in the conducting airways of that lobe. Deposition fraction is plotted against fiber diameter for a fiber aspect ratio of 10. All deposition curves exhibit a similar pattern and resemble that of deposition in the alveolar region. Deposition in the RD and LA lobes is significantly higher than

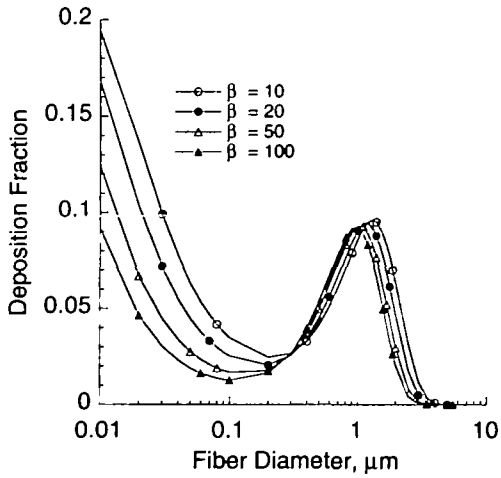

FIG. 2. Fraction of particles entering the trachea that deposited in the alveolar region for a tidal volume of 1.67 cm^3 and breathing frequency of 150 min^{-1}. Fiber density was 3.37 g/cm^3.

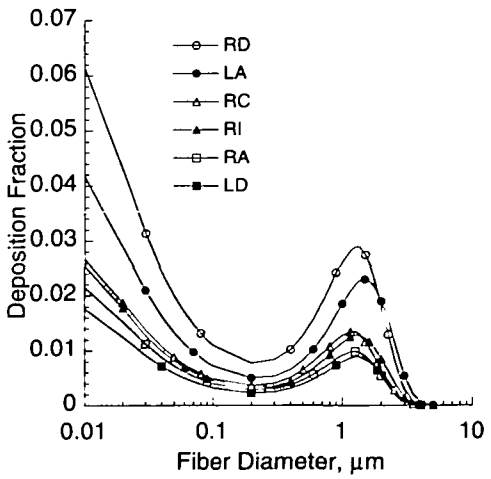

FIG. 4. Deposition fraction of fibers in each lobe of the lung for a tidal volume of 1.67 cm^3, and a breathing frequency of 150 min^{-1}. Fiber aspect ratio was 10, and fiber density was 3.37 g/cm^3.

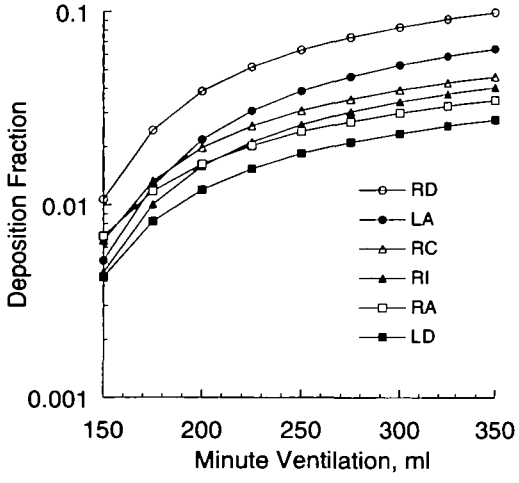

FIG. 5. Variation of lobar deposition fraction with the rat's minute ventilation for a tidal volume of 1.67 cm^3 and breathing frequency of 150 min^{-1}. Fiber diameter was 1 μm, fiber aspect ratio was 10, and fiber density was 3.37 g/cm^3.

that in other lobes. These lobes would therefore be the preferred lobes for measuring the amount of fibers deposited following an inhalation study, since they are predicted to contain more fibers than the other lobes.

The deposition fraction of fibers with $d_f = 1$ μm, $\beta = 10$, in each lobe of the rat lung as a function of the animal's minute ventilation is shown in Fig. 5. Deposition fraction increases with increasing minute ventilation. There is a 10-fold increase in deposition when the minute ventilation is increased from 150 to 350 ml. Figure 5 illustrates the significance of using accurate breathing parameters in model calculations when the values are being compared with experimental data.

More detailed deposition calculations are possible with a multiple-path model. One such calculation for the deposition fraction of fibers entering the trachea in various acini of the rat lung is presented in Fig. 6. Since there are 2404 terminal airways and thus 2404 acini in the model, one can determine the distribution of dose among different acini. If significant variation in deposition among the acini is observed, lung injury or disease in sites with high deposition may occur, even though the average acini deposition may not be high enough to warrant such occurrence. In Fig. 6, the number of acini receiving similar doses is plotted against deposition fraction per acinus. Calculations are performed for fiber diameters of 0.05, 0.2, 1, and 2 μm at an aspect ratio of 10. When fiber diameter is near 0.2 μm, a very narrow distribution is observed, which indicates similar doses among various acini. Fiber deposition in the pulmonary region approaches a minimum value near 0.2 μm diameter (see Fig. 2). Thus when pulmonary deposition is at its minimum, all acini receive similar depositions of fibers. As fiber diameter increases or decreases from 0.2 μm, the fiber deposition distribution curve becomes wider, indicating greater variation of deposition among the acini. The deposited mass of fibers is significantly larger in the sedimentation range than that in the diffusion-dominated range even if the deposition fraction for the two ranges is similar. Thus if disease occurrence is directly related to the mass deposited in the acini, this will more likely occur for fiber diameters ranging from 0.1 to 2 μm (sedimentation range).

COMPARISON WITH OTHER STUDIES

Asgharian and Yu (1989) modified the single-path deposition model by assuming each lobe of the rat lung to represent an independent single path. They created a five-path model with each path going to one lobe. The model predicted regional and lobar deposition of fibers in the lung. The lung data used in their model had a symmetric structure reported by Yeh (1980). The present multiple-path model simulation is compared with their calculations for 0.2 μm diameter with $\rho = 3.37$ g/cm^3 at a lung tidal volume of 1.68 cm^3 and a breathing frequency of 98 cycles/minute. Four fiber lengths of 0.5, 1, 5, and 10 μm are selected. Head deposition was not included in the calculations. The results are shown in Figs. 7a and 7b. Both results show similar values. Our simulations show an increase in total deposition with decreasing fiber length, while the calculations of Asgharian and Yu (1989) does not show a pattern. Both models predict the deposition fraction in the RD lobe and left lung to be similar and higher than that in the other lobes. Deposition fractions in the other lobes are also similar.

Our results were also compared with experimental data in the literature. There are a number of short-duration exposure studies aimed at measuring deposition fraction of fibers in the lungs of rats. Ding *et al.* (1997) summarized these studies. Fibers used in the experiments are polydisperse. The multiple-path model was used to calculate deposition fraction of polydisperse fibers of dimensions used in those

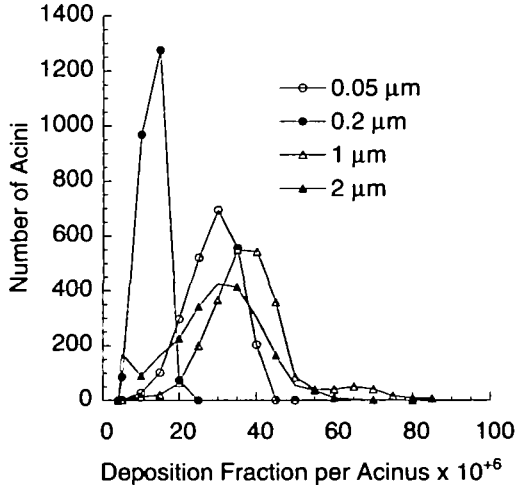

FIG. 6. Acinar dose distribution for four different fiber sizes for a tidal volume of 1.67 cm^3 and breathing frequency of 150 min^{-1}. Fiber aspect ratio was 10, and fiber density was 3.37 g/cm^3. Horizontal spacing is 2×10^{-6}.

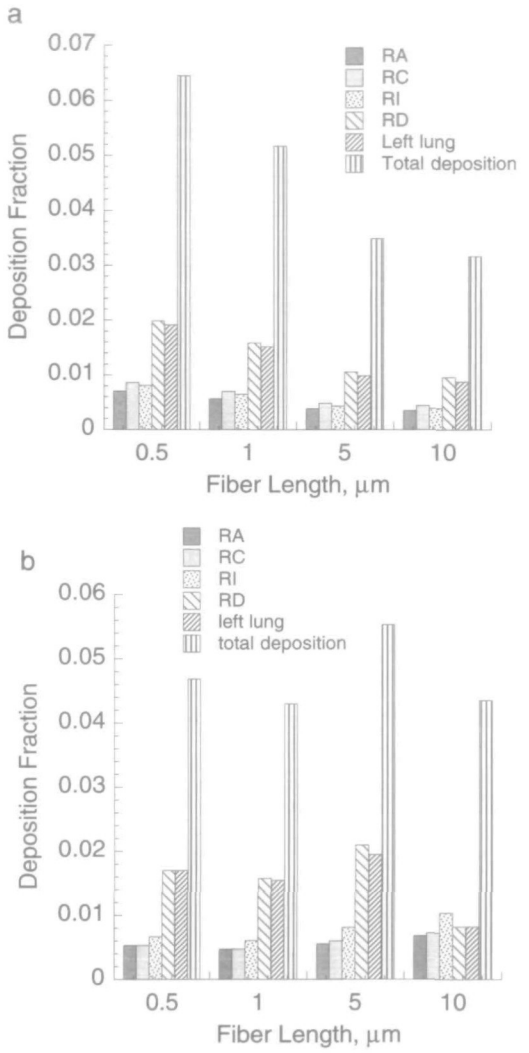

FIG. 7. Deposition fraction of fibers in the rat lung for $d_f = 0.2$ μm, $\rho = 3.37$ g/cm^3, at a lung tidal volume of 1.68 cm^3 and a breathing frequency of 98 min^{-1}. (a) Current study; (b) Asgharian and Yu (1989).

studies. Head deposition was included in the calculations. Assuming a polydisperse fiber with independent log-normal length and diameter distributions, the mass fraction of the fibers deposited in a given region of the lung, η_m, is calculated from the expression

$$\eta_m = \frac{\int_0^\infty \int_0^\infty \eta(d_f, l_f) d_f^2 l_f f(d_f) g(l_f) d(d_f) d(l_f)}{\int_0^\infty \int_0^\infty d_f^2 l_f f(d_f) g(l_f) d(d_f) d(l_f)}, \quad (24)$$

where η is the number fraction of deposition of a monodisperse fiber of diameter d_f and length l_f and $f(d_f)$ and $g(l_f)$ are the size distributions for diameter and length, respectively.

$$f(d_f) = \frac{1}{\sqrt{2\pi} d_f \ln(\sigma_{gd})} \exp\left\{-\frac{(\ln d_f - \ln \bar{d}_f)^2}{2\ln^2(\sigma_{gd})}\right\} \quad (25)$$

$$g(l_f) = \frac{1}{\sqrt{2\pi} l_f \ln(\sigma_{gl})} \exp\left\{-\frac{(\ln l_f - \ln \bar{l}_f)^2}{2\ln^2(\sigma_{gl})}\right\}, \quad (26)$$

where $\bar{d}_f$ and $\bar{l}_f$ are count mean diameter and length, and σ_{gd} and σ_{gl} are the geometric standard deviation for diameter and length.

The comparison between model prediction and experimental data for fibers depositing in the lower respiratory tract or pulmonary region is given in Fig. 8. The experimental deposition fraction in each study is plotted against the calculated deposition fraction. The dashed line in Fig. 8 indicates identical values between the experimental data and model predictions and thus a perfect agreement. The agreement between the two results is reasonable considering the uncertainty regarding the lung structure and minute ventilation used in the calculations.

CONCLUSIONS

An asymmetric, multiple-path model was used to predict deposition of fibers in the lungs of rats. The model prediction compared favorably with other model predictions and experimental data. The model has the capability of predicting site-specific deposition in the respiratory tract. It can predict deposition per acini, lobes, or regions of the lung. The effects of fiber dimensions, breathing rates, and variation of deposition among different lobes of the lung can be studied. By determining the appropriate fiber sizes to produce the target dose, the model will aid in improving the design and conduct of inhalation studies.

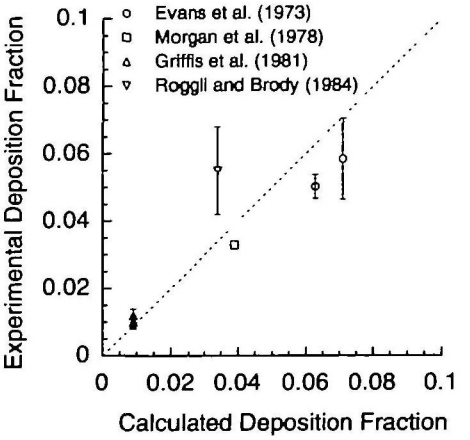

FIG. 8. The comparison of the calculated deposition fraction of fibers in the lower respiratory tract or pulmonary region of the rat lung with experimental data.

ACKNOWLEDGMENTS

This work was supported in part by grants from the North American Insulation Manufacturers Association and the Refractory Ceramic Fiber Coalition. The authors are also grateful to Dr. Barbara Kuyper for her editorial assistance in the preparation of the manuscript.

REFERENCES

Anjilvel, S., and Asgharian, B. (1995). A multiple-path model of particle deposition in the rat lung. *Fundam. Appl. Toxicol.* **28,** 41–50.

Asgharian, B. (1988). *Theoretical Deposition of Fibrous Particles in the Respiratory System of Humans and Rats.* Ph.D. thesis, State University of New York at Buffalo.

Asgharian, B., and Yu, C. P. (1988). Deposition of inhaled fibrous particles in the human lung. *J. Aerosol Med.* **1,** 37–50.

Asgharian, B., and Yu, C. P. (1989). Deposition of fibers in the rat lung. *J. Aerosol Sci.* **20,** 355–366.

Asgharian, B., Yu, C. P., and Gradon, L. (1988). Diffusion of fibers in a tubular flow. *Aerosol Sci. Technol.* **9,** 213–219.

Beeckmans, J. M. (1972). Deposition of ellipsoidal particles in the human respiratory tract. In *Assessment of Airborne Particles* (T.T. Mercer, P.E. Morrow, and M. Stober, Eds.). Thomas, Springfield, IL.

Cai, F. S., and Yu, C. P. (1988). Inertial and interceptional deposition of spherical particles and fibers in a bifurcating airway. *J. Aerosol Sci.* **19,** 679–688.

Coin, P., Roggli, V. L., and Brody, A. R. (1992). Deposition, clearance, and translocation of chrysotile asbestos from peripheral and central region of the rat lung. *Environ. Res.* **58,** 97–116.

Ding, J. Y., Yu, C. P., Zhang, L., and Chen, Y. K. (1997). Deposition modeling of fibrous particles in rats: Comparisons with available experimental data. *Aerosol Sci. Technol.* **26,** 403–414.

Evans, J. C., Evans, R. J., Holmes, A., Hounam, R. F., Jones, D. M., Morgan A., and Walsh, M. (1973). Studies on the deposition of inhaled fibrous material in the respiratory tract of rat and its subsequent clearance using radioactive trace techniques (I. UICC crocidolite asbestos). *Environ. Res.* **6,** 180–201.

Griffis, L. C., Henderson, T. R., and Pickrell, J. A. (1981). A method for determining glass in rat lung after exposure to a glass fiber aerosol. *Am. Ind. Hyg. Assoc. J.* **42,** 566–569.

Harris, R. L., and Fraser, D. A. (1976). A model for deposition of fibers in the human respiratory system. *Am. Ind. Hyg. Assoc. J.* **37,** 73–89.

Ingham, D. B. (1975). Diffusion of aerosols from a stream flowing through a cylindrical tube. *Aerosol Sci.* **6,** 125–132

Morgan, A., Talbot, R. J., and Holmes, A. (1978). Significance of fiber length in the clearance of asbestos fibers from the lung. *Bri. J. Ind. Med.* **35,** 146–153.

Raabe, O. G., Yeh, H. C., Newton, G. J., Phalen, R. F., and Velasquez, D. J. (1977). *Deposition if Inhaled Monodisperse Aerosols in Small Rodents, in Inhaled Particles IV* (W. H. Walton , B. McGovern, Eds.), Part I, pp.1–21. Pergamon Press, Oxford.

Roggli, V. L., and Brody, A. R. (1984). Changes in numbers and dimensions of chrysotile asbestos fibers in lungs of rats following short-term exposure. *Exp. Lung Res.* **7,** 133–147.

Yeh, H. C. (1980). *Respiratory Tract Deposition Models.* Inhalation Toxicology Research Institute, Lovelace Biomedical and Environmental Research Institute, Albuquerque, NM.

Yeh, H.-C., Schum. G. M., and Duggan, M. T. (1979). Anatomical models of the tracheobronchial and pulmonary regions of the rat. *Anat Rec.* **196,** 483–492.

Wang, C. S. (1975). Gravitational deposition of particles from laminar flows in inclined channels. *J. Aerosol Sc.* **6,** 191–204.

Yu, C. P. (1978). Exact analysis of aerosol deposition during steady breathing. *Powder Technol.* **21,** 55–62.

Zhang, L., and Yu. C. P. (1993). Empirical equations for nasal deposition of inhaled particles in small laboratory animals and humans. *Aerosol Sci. Technol.* **19,** 51–56.